

Andreev Reflection in the Quantum Hall Regime at an Al/InAs Junction on a Cleaved Edge

Takafumi Akiho,* Hiroshi Irie, Yusuke Nakazawa, Satoshi Sasaki, Norio Kumada, and Koji Muraki
NTT Basic Research Laboratories, NTT Corporation, 3-1 Morinosato-Wakamiya, Atsugi 243-0198, Japan
(Dated: August 30, 2024)

We have fabricated a superconductor/semiconductor (S/Sm) junction composed of Al and InAs using cleaved edge overgrowth. By exploiting the unique geometry with a thin Al/Pt/Al trilayer formed on the side surface of an in-situ cleaved heterostructure wafer containing an InAs quantum well, we achieve a superconducting critical field of ~ 5 T, allowing superconductivity and quantum Hall (QH) effects to coexist down to Landau-level filling factor $\nu = 3$. Andreev reflection at zero magnetic field shows a conductance enhancement that is limited solely by the Fermi velocity mismatch, demonstrating a virtually barrier-free, high-quality S/Sm junction. Bias spectroscopy in the QH regime reveals the opening of a superconducting gap, with the reduced downstream resistance demonstrating that the electron-hole Andreev conversion probability consistently exceeds 50%. Our results, obtained in a new experimental regime characterized by a clean edge-contacted junction with a superconducting electrode narrower than the coherence length, open new avenues for both theoretical and experimental studies of the interplay between superconductivity and QH effects and the engineering of exotic quasiparticles.

There have been ongoing efforts to realize topological superconductivity, which is expected to support exotic quasiparticles that obey non-Abelian statistics, a crucial building block for fault-tolerant quantum computation [1–6]. Among the various proposals to engineer topological superconductivity by exploiting the proximity coupling with *s*-wave superconductors, those based on quantum Hall (QH) systems [7–9] are unique in that they hold the promise of otherwise unavailable universal quantum computation using parafermions predicted in the fractional QH regime. This has led to a renewed interest and experimental efforts [10–23] in superconductor/semiconductor (S/Sm) junctions in the QH regime, despite the experimental challenges posed by the requirements of junction transparency and the coexistence of high magnetic fields and superconductivity, which are generally incompatible with each other.

Superconducting correlation is induced in QH edge channels by Andreev processes, where electrons entering the junction exit as holes, transmitting Cooper pairs into the superconductor. Experiments on NbN/graphene junctions in the integer [12] and fractional [18] QH regimes have demonstrated crossed Andreev reflection, in which electron-hole conversion takes place between counterpropagating edge channels through a narrow strip of superconductor in between. There, the negative resistance in the downstream of the junction (R_d) provided evidence of electron-hole conversion. In contrast, for a 600-nm-wide MoRe/graphene junction along a single edge, R_d was observed to oscillate or fluctuate between positive and negative as the magnetic field or gate voltage was swept [16, 20]. It was then argued that these oscillations arise from the interference of chiral Andreev edge states (CAESs), hybrid eigenmodes of electron- and hole-like edge states formed along the proximitized region [24, 25]. However, subsequent theoretical investigations have raised interfacial disorder [26], vortices [27], disorder [28], and supercurrent [29] in the superconductor, and the geometry of the junction [30] as necessary ingredients to explain the experimental observations. On the other hand, an experiment for a 150- μ m-wide NbTiN/InAs junction found negative R_d with-

out oscillations [19]. These clearly show the need for further experiments with a controlled setup to understand even the most fundamental process of Andreev conversion.

Common to the reported superconducting junctions in the QH regime [10–14, 16, 18–21, 31–33] is that they use type-II superconductors to sustain superconductivity at high fields and etching to fabricate the junction, both of which make it challenging to form a pristine and uniform junction free of interfacial disorder or in-gap states. Nonuniform interfaces would result in an inhomogeneous induced gap, leading to a soft gap [34], where in-gap states act as a source of unwanted quasiparticle tunneling into the superconductor. On the other hand, successful formation of pristine S/Sm junctions by in-situ epitaxial growth of a superconductor on the surface of a semiconductor has been reported [35–39]. In particular, epitaxial junctions of Al and InAs nanowires [40] or two-dimensional electron systems (2DEGs) [41] have been shown to have a hard superconducting gap free of in-gap states. Although Al is a type-I superconductor, in thin films it can maintain superconductivity up to a few tesla when the field is in the plane of the film, a property that has been exploited for hybrid nanowires. Furthermore, by adding heavy elements with strong spin-orbit coupling such as Pt, the in-plane critical field can be increased to a several tesla [42, 43]. However, despite their superior properties, epitaxial Al/InAs junctions could not be used for QH systems, because the field must be applied perpendicular to the 2DEG, i.e., to the superconducting film.

Here, we overcome this limitation by using a novel geometry in which the superconducting thin film is grown on the side surface of a semiconductor wafer, and realize an Al/InAs epitaxial junction that operates in the QH regime. Using the cleaved edge overgrowth (CEO) technique [44], we deposited an Al/Pt/Al trilayer on an in-situ cleaved edge surface of a wafer containing an InAs quantum well (QW). Andreev reflection at zero field indicates that the conductance enhancement is limited solely by the Fermi velocity mismatch, demonstrating a high-quality junction that is virtually free of an interface barrier. At high fields, we observe that R_d is reduced near zero bias in the plateau regions for filling factors

from 10 to 3, indicating that the probability of electron-hole conversion consistently exceeds 50%, without oscillatory behavior. The geometry of our experiment is unique in that 1) the field direction, being parallel to the plane of the thin superconductor, eliminates vortices, and 2) the 2DES is directly edge-contacted by the superconductor, with no spatial overlap along the field direction. The observation of Andreev conversion with a clear bias dependence in the unique geometry provides new insights into the underlying processes. In addition, our approach to fabricating etch-free, high-quality superconducting junctions will open a new avenue for the study of engineered topological superconductivity.

Our CEO device was fabricated from a heterostructure wafer grown on a GaSb(001) substrate. (See Supporting Information (SI) for the layer structure.) The wafer, cut into a $14 \text{ mm} \times 15 \text{ mm}$ piece, was thinned to $300 \text{ }\mu\text{m}$ by polishing to facilitate cleaving and thus obtain a flat cleaved edge surface. The wafer was mounted at 90° on a Mo sample holder and was cleaved in UHV ($< 5.0 \times 10^{-10}$ mbar) using a wobble stick. The wafer was then transferred under UHV to the deposition chamber, where a superconducting electrode was deposited on the cleaved edge surface, with the sample holder cooled by direct contact with a liquid nitrogen cold plate, a crucial step for obtaining epitaxial Al layers [35]. We used photolithography to process the sample into a gate-defined Hall bar with normal Ti/Au electrodes and an S/Sm junction at the cleaved edge. (See SI for fabrication details.) Measurements were conducted in a ^3He cryostat equipped with a superconducting vector magnet. The 2DES density and mobility are $n = 3.0 \times 10^{15} \text{ m}^{-2}$ and $\mu = 63 \text{ m}^2/\text{Vs}$, respectively.

Figure 1(a) shows a schematic of our CEO device. The Hall bar is defined electrostatically by applying a negative voltage $V_{\text{FG}} (\lesssim -1.2 \text{ V})$ to the front gate and depleting the 2DES beneath [45]. The front gate has an opening above the cleaved edge, defining a narrow junction of width L , nominally $3\text{-}\mu\text{m}$ wide, between the superconductor (#8) and the 2DES. The scanning electron microscope (SEM) image taken near the narrow junction of a dummy sample confirms the formation of a split gate [Fig. 1(b)]. The superconductor (#8) was electrically accessed through the wide S/Sm junctions on either side, using the 2DES regions isolated from the Hall bar by the front gate as leads and the Ti/Au contacts #6 and #7 as current and voltage probes, respectively [46]. We applied AC and DC bias (I) from the drain electrode #6.

Figure 1(c) presents the longitudinal (R_{xx}) and Hall (R_{xy}) resistances of the device, measured in a perpendicular field B_z using normal contacts, showing well-developed QH effects at Landau-level filling factor $\nu (= nh/eB_z)$ of 3 to 10, where h is Planck's constant and e is the elementary charge. Figure 1(d) shows the superconducting property of the Al/Pt/Al film of a control sample fabricated on the cleaved edge of a semi-insulating GaAs(100) substrate. The two-terminal resistance R of an Al/Pt/Al trilayer of thicknesses 6, 1, and 2 nm from bottom to top is plotted as a function of the field B_z applied perpendicular to the substrate (i.e., parallel to the super-

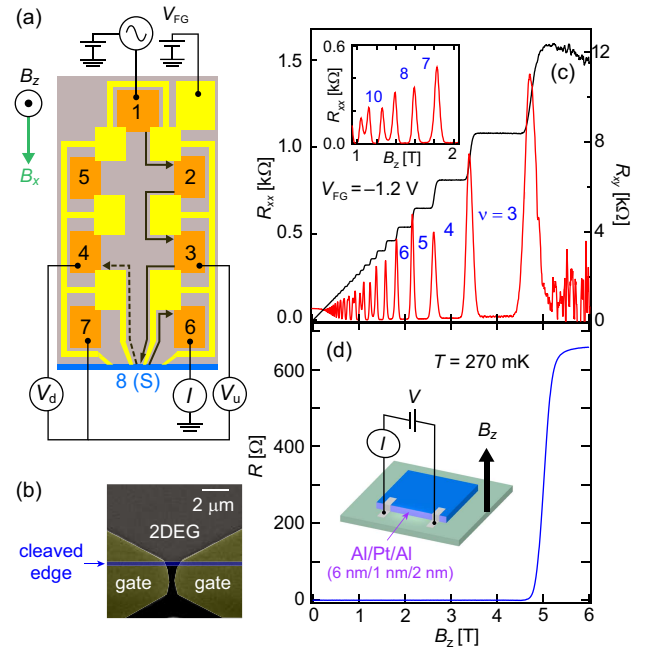


FIG. 1. (a) Schematic representation of the device and the measurement setup. #1 through #7 and #8 represent normal and superconducting electrodes, respectively. The black solid and dashed lines with arrows indicate the direction of the edge channels under a perpendicular magnetic field B_z . (b) SEM image of the S/Sm interface at the cleaved edge of a dummy sample. (c) Magnetic field dependence of R_{xx} (red) and R_{xy} (black) measured using normal contacts. The inset shows a magnified view of R_{xx} at low fields. (d) Magnetic field dependence of the resistance of a control Al/Pt/Al sample. The inset shows a schematic of the measurement setup. The magnetic field is applied parallel to the Al/Pt/Al film.

conducting thin film). The critical in-plane field B_c^{\parallel} is $\sim 5 \text{ T}$ for the 6/1/2-nm trilayer, which decreased as the bottom Al thickness increased. Based on this result, we employed the 6/1/2-nm trilayer structure for the S/Sm junction. The results in Figs. 1(c) and (d) together confirm that, below $B_z = 5 \text{ T}$, superconductivity and QH effects can coexist in our device employing an Al superconductor.

Now we characterize the S/Sm junctions by measuring the differential resistance at $B_z = 0 \text{ T}$ using the setup shown in Fig. 1(a). Here, we focus on the results for $R_d^0 = dV_d/dI$ obtained with contacts #4 and #7, while those for $R_u^0 = dV_u/dI$ obtained with contacts #3 and #7 are provided in SI. Figures 2(a) show the DC bias (V_{dc}) dependence of R_d^0 at different temperatures [47]. A pronounced zero-bias minimum is observed at low temperatures, demonstrating Andreev reflection, i.e., reflection of an incident electron from the 2DES as a hole, thereby enhancing the conductance [48]. From the temperature at which the zero-bias minimum evolves into a broad maximum, the critical temperature T_c is determined to be 1070 mK, with the corresponding BCS gap $\Delta = 1.764k_B T_c$ of $163 \text{ }\mu\text{eV}$, where k_B is the Boltzmann constant.

To characterize the S/Sm junction more quantitatively, we evaluate the Andreev reflection probability. To this end, we

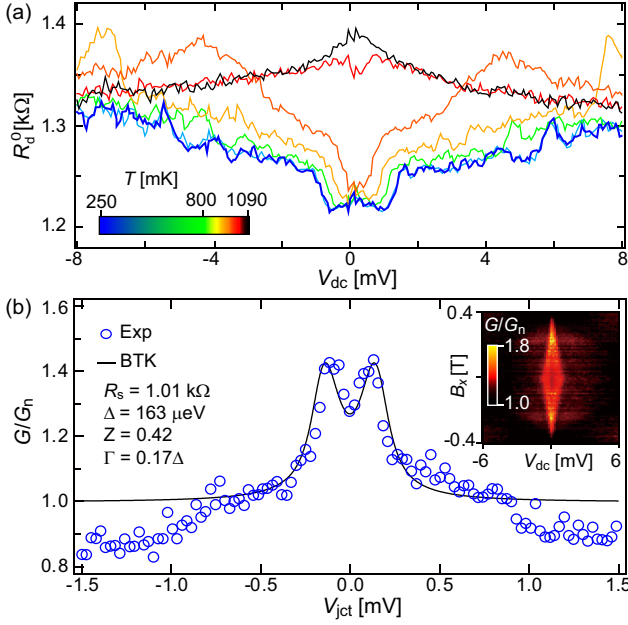


FIG. 2. (a) DC bias dependence of the differential resistance at zero magnetic field and at different temperatures. (b) Bias dependence of the differential conductance, normalized to the value outside the superconducting gap. Note that the horizontal axis represents the voltage across the junction $V_{\text{jct}} \equiv (\Delta/e)V_{\text{dc}}/V_{\Delta}$ (see main text for details). The solid line represents a fit using the BTK model. (Inset) Normalized differential conductance as a function of V_{dc} and B_x , with the magnetic field B_x applied perpendicular to the superconducting film.

derived the differential conductance of the junction, $G = (R_d^0 - R_s)^{-1}$, by subtracting the series resistance R_s from R_d^0 . We estimated $R_s = 1.01$ k Ω by noting that the voltage drop across the S/Sm junction (V_{jct}) equals Δ/e at the DC bias (V_{Δ}) for which the Fermi level in the normal region coincides with the superconducting gap edge at base temperature. Figure 2(b) plots the normalized differential conductance G/G_n as a function of $V_{\text{jct}} \equiv (\Delta/e)V_{\text{dc}}/V_{\Delta}$, where G_n is the differential conductance at a finite bias outside the superconducting gap. The solid line represents a fit based on the modified Blonder-Tinkham-Klapwijk (BTK) model described by [12, 49–51],

$$G/G_n = C \int_{-\infty}^{\infty} [f(E - eV) - f(E)](1 + A - B)dE. \quad (1)$$

Here, C is a constant, E is the energy, f is the Fermi distribution function, and $A = A(E, \Delta, Z, \Gamma)$ and $B = B(E, \Delta, Z, \Gamma)$ are the Andreev and normal reflection probabilities, respectively [52]. Z is a dimensionless parameter characterizing the effective barrier at the S/Sm interface, and Γ , which enters A and B as the imaginary part of the energy, describes the lifetime broadening.

As shown in Fig. 2(b), $Z = 0.42$ and $\Gamma = 0.17\Delta$ reproduce the measured bias dependence, including the conductance enhancement factor G/G_n of 1.28 at zero bias. Both finite Z and Γ reduce the Andreev reflection probability, resulting in a conductance enhancement factor less than 2, the value ex-

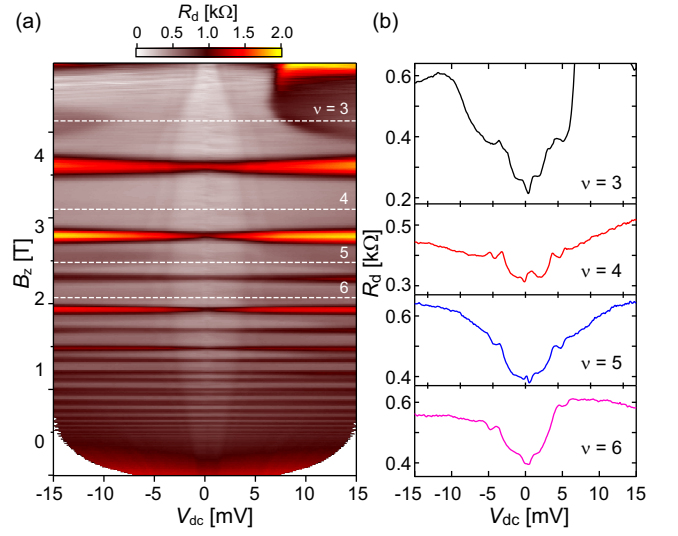


FIG. 3. (a) Color scale plot of R_d as a function of V_{dc} and B_z . (b) Line cuts of the data in (a) at $\nu = 3, 4, 5,$ and 6 .

pected for an ideal junction. Note, however, that a mismatch in the Fermi velocity at the junction leads to a finite normal reflection probability even in the absence of a barrier. The resulting I - V characteristics can be described by replacing Z with an effective value $Z_{\text{eff}} = \sqrt{Z^2 + (1-r)^2}/4r$, where r is the Fermi velocity ratio [53]. In fact, for our InAs 2DES with $v_F = 5 \times 10^5$ m/s, the Fermi velocity mismatch alone is sufficient to make $Z_{\text{eff}} \geq 0.42$, assuming bulk Al [54]. Including the two-dimensionality of the 2DES, which is not considered in the BTK model, would further increase Z_{eff} [55]. These observations suggest that our junction is virtually barrier-free. Interestingly, the obtained $\Gamma = 0.17\Delta$ corresponds to a quasiparticle lifetime $\tau_{\text{qp}} (= h/2\pi\Gamma)$ of 24 ps. This is more than 10 times longer than that for the NbN/graphene device [12], indicating that a high-quality superconducting electrode has been obtained by CEO.

We also measured Andreev reflection with the magnetic field B_x applied perpendicular to the superconducting thin film [inset of Fig. 2(b)]. From the critical field of $B_c^{\perp} = 0.39$ T, the effective coherence length is estimated to be $\xi = 29$ nm. While this value is much shorter than the typical coherence length for Al (> 1 μm), possibly due to the spin-orbit scattering induced by Pt, it is important to note that the thickness of our superconducting film (10 nm) is even smaller.

We next study the Andreev reflection in the QH regime by applying a magnetic field B_z perpendicular to the 2DES (i.e., parallel to the superconducting thin film). Figure 3(a) plots R_d , the resistance measured on the edge channels downstream of the S/Sm junction, as a function of V_{dc} and B_z . The plot reveals a region of reduced R_d around $V_{\text{dc}} = 0$ V, which narrows above 4 T but remains open up to 4.8 T. We associate this with the superconducting gap [56]. Figure 3(b) displays horizontal line cuts of Fig. 3(a) at several integer values of ν , showing reduced R_d inside the superconducting gap. We emphasize

that such a clear bias dependence, indicating a superconducting gap in the QH regime, has not been previously reported for junctions along a single edge [57]. We first notice that although R_d is clearly reduced around zero bias, it remains positive. This contrasts with the sign-oscillating R_d reported for MoRe/graphene junctions [16, 20], where negative R_d indicates electron-hole conversion. We note that in our data R_d is finite outside the superconducting gap. This indicates that the coupling between the edge channels and the Al electrode is imperfect; that is, even in the absence of superconductivity, some fraction of electrons in the upstream channels are transferred to the downstream channels. As we show below, this effect can be incorporated into a Landauer-Büttiker-type model, from which the probability P_h of electron-hole conversion by the Andreev process can be derived.

We construct a Landauer-Büttiker-type model appropriate for our device layout involving a superconducting electrode. The current-voltage relation can be expressed as $\mathbf{I} = \nu G_0 \mathbf{M} \mathbf{V}$, where $G_0 = e^2/h$ is the conductance quantum, and $\mathbf{I} = (\dots, I_i, \dots)^T$ and $\mathbf{V} = (\dots, V_i, \dots)^T$ with I_i (V_i) the current (voltage) of the i th contact ($i = 1, 3, 4, 6, 7, 8$). (Contacts #2 and #5, which are not used in the $R_{d(u)}$ measurements, are excluded.) \mathbf{M} is the normalized conductance matrix. The effect of imperfect edge coupling is accounted for by introducing a parameter T_i . As shown schematically in the inset of Fig. 4, a portion of the electrons in the incoming ν edge channels are reflected before reaching the superconducting electrode #8 with probability $1 - T_i$ and fed into the outgoing channels. The definition of P_h is such that the injection of an electron into the junction results in the emission of, on average, P_h holes into the outgoing channels. That is, $P_h = 1$ and 0 correspond to 100% electron-hole conversion (i.e., perfect Cooper-pair transmission) and perfect normal reflection (i.e., no current through the junction), respectively. $P_h = 0.5$ means that on average these two events occur with equal probability. Thus, the matrix \mathbf{M} is given as

$$\mathbf{M} = \begin{pmatrix} 1 & 0 & -1 & 0 & 0 & 0 \\ -1 & 1 & 0 & 0 & 0 & 0 \\ 0 & \eta - 1 & 1 & 0 & 0 & -\eta \\ 0 & 0 & 0 & \eta' & 0 & -\eta' \\ 0 & 0 & 0 & 0 & \eta' & -\eta' \\ 0 & -\eta & 0 & -\eta' & -\eta' & \eta + 2\eta' \end{pmatrix}, \quad (2)$$

where $\eta \equiv 2T_i P_h$ and η' is the counterpart of η for the wide junctions connected to contacts #6 and #7. By solving $\mathbf{I} = \nu G_0 \mathbf{M} \mathbf{V}$ for \mathbf{V} with $\mathbf{I} = (-I, 0, 0, I, 0, 0)^T$, we obtain [58]

$$R_d \equiv \frac{V_4 - V_7}{I} = \left(\frac{1}{2T_i P_h} - 1 \right) \frac{1}{\nu G_0}, \quad (3)$$

$$R_u \equiv \frac{V_3 - V_7}{I} = \frac{1}{2T_i P_h} \frac{1}{\nu G_0}. \quad (4)$$

Note that for $T_i < 1$, R_d becomes negative only when $P_h > 1/2T_i$, even if $P_h > 0.5$.

We deduced T_i at each integer ν from the measured R_d and R_u outside the superconducting gap ($V_{dc} = -10$ mV) by setting $P_h = 0.5$ in Eqs. (3) and (4). As shown in the upper panel

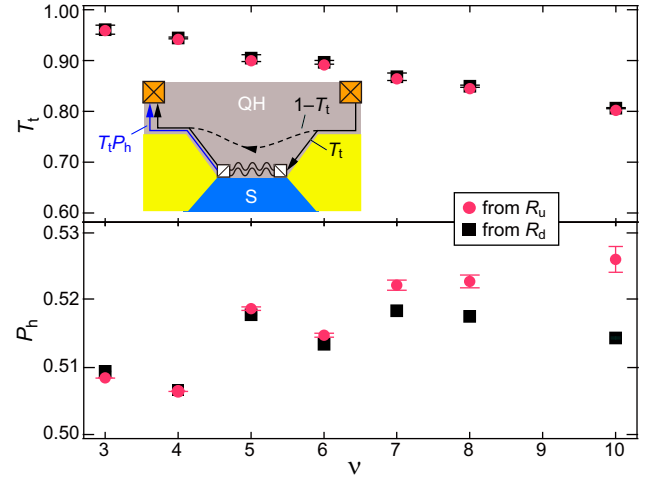


FIG. 4. ν dependence of T_i (upper panel) and P_h (lower panel). The plots show results derived separately from R_d and R_u using Eqs. (3) and (4), respectively. The inset shows a schematic of the processes involved in our Andreev reflection measurement in the QH regime. The black solid lines indicate the flow of electrons entering and exiting the S/QH junction. The dashed line schematically shows the path of electrons traveling downstream without impinging on the junction. The wavy lines depict CAESs, while the blue line illustrates the flow of holes converted from electrons through the CAESs.

of Fig. 4, R_d and R_u give consistent results, both showing that T_i gradually increases from 0.8 to 0.96 as ν decreases from 10 to 3. We used these T_i values to derive P_h from R_d and R_u at $V_{dc} = 0$ mV. As shown in the lower panel of Fig. 4, R_d and R_u give similar results, showing that P_h consistently exceeds 0.5.

Two main aspects of our results need to be discussed: the absence of oscillatory behavior in R_d and the preferential reflection of holes, indicated by $P_h > 0.5$. Theories predict that, for an ideal junction without disorder, P_h should oscillate as a function of junction width L [28, 59, 60] and bias [27, 61], due to the interference between CAESs, reflecting their momentum difference. On the other hand, it is also argued that the oscillations will only be visible at specific magnetic fields per Landau level; away from these fields, the oscillation amplitude will rapidly decay, causing P_h to average out to 0.5 [28]. The absence of such field dependence in the reported experiment [16] is a key aspect that triggered the subsequent theoretical investigations [26–30]. In our data, R_d (and hence P_h) remains nearly constant within each QH plateau, maintaining $P_h > 0.5$, without oscillations or sharp field dependence. One could speculate on the reasons for the absence of oscillations, such as the involvement of multiple edge channels or factors like temperature, momentum difference, or junction width being inadequate for resolving the interference. However, in either case, the question arises as to why P_h does not average out to 0.5. The absence of sharp field dependence also remains unexplained.

Turning to the result in Fig. 4(b), P_h gradually increases with increasing ν (i.e., decreasing B_z). No clear difference in P_h is observed between the odd and even ν , where the in-

coming edge channels are partially spin-polarized and unpolarized, respectively. This suggests the presence of a spin-flip mechanism, likely due to the spin-orbit interaction in the Pt layer.

Another notable feature in our data is the absence of discontinuous jumps in R_d during magnetic field sweeps, which were reported for MoRe/graphene junctions and attributed to a phase shift in Δ resulting from vortices hopping in and out of the superconductor [16, 20]. In our setup, the superconductor is thinner than the coherence length, and we utilize a two-axis vector magnet to align the magnetic field parallel to the film. This minimizes the possibility of vortices playing any role, consistent with the absence of discontinuous jumps. In an attempt to account for the $P_h > 0.5$ observed in their 150- μm -wide NbTiN/InAs junction, the authors of Ref. [19] speculated that electrons may have a higher probability than holes to tunnel into the superconductor. Although the origin of such asymmetry, if present, is unclear, the absence of vortices, which promote electron/hole tunneling into the superconductor, makes this scenario less likely in our CEO device. While the effects of vortices have been studied from different theoretical perspectives [27, 28], the irrelevance of vortices in our CEO device is expected to help elucidate the mechanism of Andreev conversion in the QH regime.

The narrowness of the superconducting electrode can affect the Andreev processes in several additional ways. These include the guiding center of the electron and hole orbits comprising the CAESs [24, 25, 28], confinement-induced quantization in the superconductor [62, 63], and the spatial distribution of the screening supercurrent. Furthermore, the much smaller Δ of Al compared to those in previous studies would affect the velocity of CAESs and their momentum difference. These factors place our experiment in a unique regime, distinct from previous ones. On the other hand, it is argued that the scattering properties at the endpoints of the junction play a key role in determining the electron-hole conversion probability, which, however, cannot be adequately accounted for by one-dimensional models [30]. Two-dimensional models that properly incorporate the above effects will be necessary to understand the observed behavior. Our observation of $P_h > 0.5$ along with a clear bias dependence in a unique setup will thus stimulate further theoretical and experimental investigations.

In summary, using cleaved edge overgrowth, we have successfully fabricated a clean, virtually barrier-free Al/InAs junction that operates in the QH regime. Thanks to the high interface quality, we observed the opening of a superconducting gap in bias spectroscopy up to 4.8 T in the QH regime—a behavior previously unseen in junctions along a single edge. The reduced downstream resistance within the superconducting gap indicates an electron-hole Andreev conversion probability consistently exceeding 50%. Our results, obtained in a unique setup where the 2DES is directly edge-contacted by a superconducting electrode narrower than the coherence length, are expected to stimulate further theoretical investigations into the processes involved in Andreev conversion. Our demonstration of an epitaxial S/QH junction utilizing Al, a

significantly cleaner superconductor, opens new avenues for exploring non-Abelian quasiparticles, with substantial implications for both experimental and theoretical advancements in nanoscience.

The authors thank H. Murofushi for device processing, M. Imai for drawing support, H. Kamata for measurement advice, and T. Wakamura for discussions on Andreev reflection data.

* takafumi.akiho@ntt.com

- [1] L. Fu and C. L. Kane, “Superconducting proximity effect and Majorana fermions at the surface of a topological insulator,” *Phys. Rev. Lett.* **100**, 096407 (2008).
- [2] Y. Oreg, G. Refael, and F. von Oppen, “Helical liquids and Majorana bound states in quantum wires,” *Phys. Rev. Lett.* **105**, 177002 (2010).
- [3] R. M. Lutchyn, J. D. Sau, and S. Das Sarma, “Majorana fermions and a topological phase transition in semiconductor-superconductor heterostructures,” *Phys. Rev. Lett.* **105**, 077001 (2010).
- [4] M. Leijnse and K. Flensberg, “Introduction to topological superconductivity and Majorana fermions,” *Semicond. Sci. Technol.* **27**, 124003 (2012).
- [5] J. Alicea, “New directions in the pursuit of Majorana fermions in solid state systems,” *Rep. Prog. Phys.* **75**, 076501 (2012).
- [6] K. Flensberg, F. von Oppen, and A. Stern, “Engineered platforms for topological superconductivity and Majorana zero modes,” *Nat. Rev. Mater.* **6**, 944–958 (2021).
- [7] R. S. K. Mong, D. J. Clarke, J. Alicea, N. H. Lindner, P. Fendley, C. Nayak, Y. Oreg, A. Stern, E. Berg, K. Shtengel, and M. P. A. Fisher, “Universal topological quantum computation from a superconductor-abelian quantum Hall heterostructure,” *Phys. Rev. X* **4**, 011036 (2014).
- [8] D. J. Clarke, J. Alicea, and K. Shtengel, “Exotic non-Abelian anyons from conventional fractional quantum Hall states,” *Nat. Commun.* **4**, 1348–1349 (2013).
- [9] D. J. Clarke, J. Alicea, and K. Shtengel, “Exotic circuit elements from zero-modes in hybrid superconductor-quantum-Hall systems,” *Nat. Phys.* **10**, 877–882 (2014).
- [10] Z. Wan, A. Kazakov, M. J. Manfra, L. N. Pfeiffer, K. W. West, and L. P. Rokhinson, “Induced superconductivity in high-mobility two-dimensional electron gas in gallium arsenide heterostructures,” *Nat. Commun.* **6**, 1–5 (2015).
- [11] F. Amet, C. T. Ke, I. V. Borzenets, J. Wang, K. Watanabe, T. Taniguchi, R. S. Deacon, M. Yamamoto, Y. Bomze, S. Tarucha, and G. Finkelstein, “Supercurrent in the quantum Hall regime,” *Science* **352**, 966–969 (2016).
- [12] G. H. Lee, K. F. Huang, D. K. Efetov, D. S. Wei, S. Hart, T. Taniguchi, K. Watanabe, A. Yacoby, and P. Kim, “Inducing superconducting correlation in quantum Hall edge states,” *Nat. Phys.* **13**, 693–698 (2017).
- [13] Y. Kozuka, A. Sakaguchi, J. Falson, A. Tsukazaki, and M. Kawasaki, “Andreev reflection at the interface with an oxide in the quantum Hall regime,” *J. Phys. Soc. Jpn.* **87**, 124712 (2018).
- [14] J. Zhi, N. Kang, F. Su, D. Fan, S. Li, D. Pan, S. P. Zhao, J. Zhao, and H. Q. Xu, “Coexistence of induced superconductivity and quantum Hall states in InSb nanosheets,” *Phys. Rev. B* **99**, 245302 (2019).
- [15] S. Guiducci, M. Carrega, G. Biasiol, L. Sorba, F. Beltram, and

- S. Heun, “Toward quantum Hall effect in a Josephson junction,” *Phys. Stat. Solidi. Rapid Res. Lett.* **13**, 1800222 (2019).
- [16] L. Zhao, E. G. Arnault, A. Bondarev, A. Seredinski, T. F. Q. Larson, A. W. Draelos, H. Li, K. Watanabe, T. Taniguchi, F. Amet, H. U. Baranger, and G. Finkelstein, “Interference of chiral Andreev edge states,” *Nat. Phys.* **16**, 862–867 (2020).
- [17] D. Wang, E. J. Telford, A. Benyamini, J. Jesudasan, P. Raychaudhuri, K. Watanabe, T. Taniguchi, J. Hone, C. R. Dean, and A. N. Pasupathy, “Andreev reflections in NbN/Graphene junctions under large magnetic fields,” *Nano Lett.* **21**, 8229–8235 (2021).
- [18] Ö. Gül, Y. Ronen, S. Y. Lee, H. Shapourian, J. Zauberman, Y. H. Lee, K. Watanabe, T. Taniguchi, A. Vishwanath, A. Yacoby, and P. Kim, “Andreev reflection in the fractional quantum hall state,” *Phys. Rev. X* **12**, 021057 (2022).
- [19] M. Hatefipour, J. J. Cuozzo, J. Kanter, W. M. Strickland, C. R. Allemang, T.-M. Lu, E. Rossi, and J. Shabani, “Induced superconducting pairing in integer quantum Hall edge states,” *Nano Lett.* **22**, 6173–6178 (2022).
- [20] L. Zhao, Z. Iftikhar, T. F. Q. Larson, E. G. Arnault, K. Watanabe, T. Taniguchi, F. Amet, and G. Finkelstein, “Loss and decoherence at the quantum Hall–superconductor interface,” *Phys. Rev. Lett.* **131**, 176604 (2023).
- [21] H. Vignaud, D. Perconte, W. Yang, B. Kousar, E. Wagner, F. Gay, K. Watanabe, T. Taniguchi, H. Courtois, Z. Han, H. Sellier, and B. Sacépé, “Evidence for chiral supercurrent in quantum Hall Josephson junctions,” *Nature* **624**, 545–550 (2023).
- [22] L. Zhao, E. G. Arnault, T. F. Q. Larson, K. Watanabe, T. Taniguchi, F. Amet, and G. Finkelstein, “Nonlocal transport measurements in hybrid quantum Hall–superconducting devices,” *Phys. Rev. B* **109**, 115416 (2024).
- [23] M. Hatefipour, J. J. Cuozzo, I. Levy, W. M. Strickland, D. Langone, E. Rossi, and J. Shabani, “Andreev reflection of quantum Hall states through a quantum point contact,” *Phys. Rev. B* **109**, 035430 (2024).
- [24] H. Hoppe, U. Zülicke, and G. Schön, “Andreev reflection in strong magnetic fields,” *Phys. Rev. Lett.* **84**, 1804–1807 (2000).
- [25] F. Giazotto, M. Governale, U. Zülicke, and F. Beltram, “Andreev reflection and cyclotron motion at superconductor—normal-metal interfaces,” *Phys. Rev. B* **72**, 54518 (2005).
- [26] A. Manesco, I. M. Flór, C.-X. Liu, and A. R. Akhmerov, “Mechanisms of Andreev reflection in quantum Hall graphene,” *SciPost Physics Core* **5**, 045 (2022).
- [27] Y. Tang, C. Knapp, and J. Alicea, “Vortex-enabled Andreev processes in quantum Hall–superconductor hybrids,” *Phys. Rev. B* **106**, 245411 (2022).
- [28] V. D. Kurilovich, Z. M. Raines, and L. I. Glazman, “Disorder-enabled Andreev reflection of a quantum Hall edge,” *Nat. Commun.* **14**, 2237 (2023).
- [29] A. B. Michelsen, P. Recher, B. Braunecker, and T. L. Schmidt, “Supercurrent-enabled Andreev reflection in a chiral quantum Hall edge state,” *Phys. Rev. Res.* **5**, 013066 (2023).
- [30] A. David, J. S. Meyer, and M. Houzet, “Geometrical effects on the downstream conductance in quantum-Hall–superconductor hybrid systems,” *Phys. Rev. B* **107**, 125416 (2023).
- [31] H. Takayanagi and T. Akazaki, “Semiconductor-coupled superconducting junctions using NbN electrodes with high H_{c2} and T_c ,” *Physica B Condens. Matter* **249-251**, 462–466 (1998).
- [32] J. Eroms, D. Weiss, J. De Boeck, G. Borghs, and U. Zülicke, “Andreev reflection at high magnetic fields: Evidence for electron and hole transport in edge states,” *Phys. Rev. Lett.* **95**, 107001 (2005).
- [33] P. Rickhaus, M. Weiss, L. Marot, and C. Schönenberger, “Quantum Hall effect in graphene with superconducting electrodes,” *Nano Lett.* **12**, 1942–1945 (2012).
- [34] S. Takei, B. M. Fregoso, H.-Y. Hui, A. M. Lobos, and S. Das Sarma, *Phys. Rev. Lett.* **110**, 186803 (2013).
- [35] P. Krogstrup, N. L. B. Ziino, W. Chang, S. M. Albrecht, M. H. Madsen, E. Johnson, J. Nygård, C. M. Marcus, and T. S. Jespersen, “Epitaxy of semiconductor–superconductor nanowires,” *Nat. Mater.* **14**, 400–406 (2015).
- [36] J. Shabani, M. Kjaergaard, H. J. Suominen, Younghyun Kim, F. Nichele, K. Pakrouski, T. Stankevic, R. M. Lutchyn, P. Krogstrup, R. Feidenhans’L, S. Kraemer, C. Nayak, M. Troyer, C. M. Marcus, and C. J. Palmstrøm, “Two-dimensional epitaxial superconductor–semiconductor heterostructures: A platform for topological superconducting networks,” *Phys. Rev. B* **93**, 155402 (2016).
- [37] M. Bjergfelt, D. J. Carrad, T. Kanne, M. Aagesen, E. M. Fiordaliso, E. Johnson, B. Shojaei, C. J. Palmstrøm, P. Krogstrup, T. S. Jespersen, and J. Nygård, “Superconducting vanadium/indium–arsenide hybrid nanowires,” *Nanotechnology* **30**, 294005 (2019).
- [38] T. Kanne, M. Marnauza, D. Olsteins, D. J. Carrad, J. E. Sestoft, J. de Bruijkere, L. Zeng, E. Johnson, E. Olsson, K. Grove-Rasmussen, and J. Nygård, “Epitaxial Pb on InAs nanowires for quantum devices,” *Nat. Nanotechnol.* **16**, 776–781 (2021).
- [39] S. A. Khan, S. Martí-Sánchez, D. Olsteins, C. Lampadaris, D. J. Carrad, Y. Liu, J. Quiñones, M. C. Spadaro, T. S. Jespersen, P. Krogstrup, and J. Arbiol, “Epitaxially driven phase selectivity of Sn in hybrid quantum nanowires,” *ACS Nano* **17**, 11794–11804 (2023).
- [40] W. Chang, S. M. Albrecht, T. S. Jespersen, F. Kuemmeth, P. Krogstrup, J. Nygård, and C. M. Marcus, “Hard gap in epitaxial semiconductor–superconductor nanowires,” *Nat. Nanotechnol.* **10**, 232–236 (2015).
- [41] M. Kjaergaard, F. Nichele, H. J. Suominen, M. P. Nowak, M. Wimmer, A. R. Akhmerov, J. A. Folk, K. Flensberg, J. Shabani, C. J. Palmstrøm, and C. M. Marcus, “Quantized conductance doubling and hard gap in a two-dimensional semiconductor–superconductor heterostructure,” *Nat. Commun.* **7**, 12841 (2016).
- [42] R. Meservey and P. M. Tedrow, “Spin-polarized electron tunneling,” *Phys. Rep.* **238**, 173–243 (1994).
- [43] G. P. Mazur, N. van Loo, J.-Y. Wang, T. Dvir, G. Wang, A. Khindanov, S. Korneychuk, F. Borsoi, R. C. Dekker, G. Badawy, P. Vinke, S. Gazibegovic, E. P. A. M. Bakkers, M. Quintero-Pérez, S. Heedt, and L. P. Kouwenhoven, “Spin-mixing enhanced proximity effect in aluminum-based superconductor–semiconductor hybrids,” *Adv. Mater.* **34**, 2202034 (2022).
- [44] L. Pfeiffer, H. L. Störmer, K. W. Baldwin, K. W. West, A. R. Goñi, A. Pinczuk, R. C. Ashoori, M. M. Dignam, and W. Wegscheider, “Cleaved edge overgrowth for quantum wire fabrication,” *J. Cryst. Growth* **127**, 849–857 (1993).
- [45] This prevents non-topological edge conduction in the QH regime caused by electron accumulation at the edge, which can occur in etch-defined InAs channels [64–66]. Additionally, it allows the junction ends to be defined electrostatically, avoiding contamination or damage from direct processing.
- [46] This design was employed to access the superconductor while avoiding unintended breaks at steps on the cleaved edge and shorting to the conducting GaSb substrate.
- [47] Throughout this paper, V_{dc} is the measured DC component of V_u , the volatage between contacts #3 and #7.
- [48] A. F. Andreev, “The thermal conductivity of the intermediate state in superconductors,” *Zh. Eksp. Teor. Fiz.* **46**, 1823–1828

- (1964), [Sov. Phys. JETP **19**, 1228 (1964)].
- [49] G. E. Blonder, M. Tinkham, and T. M. Klapwijk, “Transition from metallic to tunneling regimes in superconducting micro-constrictions: Excess current, charge imbalance, and supercurrent conversion,” *Phys. Rev. B* **25**, 4515–4532 (1982).
- [50] R. C. Dynes, V. Narayanamurti, and J. P. Garno, “Direct measurement of quasiparticle-lifetime broadening in a strong-coupled superconductor,” *Phys. Rev. Lett.* **41**, 1509–1512 (1978).
- [51] Y. G. Naidyuk, R. Häussler, and H. v. Löhneysen, “Magnetic field dependence of the Andreev reflection structure in the conductivity of S-N point contacts,” *Physica B: Cond. Matter* **218**, 122–125 (1996).
- [52] $A = a^*a$ and $B = b^*b$, where $a = u_0v_0/\gamma$, $b = -(u_0^2 - v_0^2)/\gamma$, and $\gamma = u_0^2 + Z^2(u_0^2 - v_0^2)$ with $u_0^2 = \frac{1}{2} \left[1 + \frac{\sqrt{(E+i\Gamma)^2 - \Delta^2}}{E+i\Gamma} \right]$ and $v_0^2 = \frac{1}{2} \left[1 - \frac{\sqrt{(E+i\Gamma)^2 - \Delta^2}}{E+i\Gamma} \right]$.
- [53] G. E. Blonder and M. Tinkham, “Metallic to tunneling transition in Cu-Nb point contacts,” *Phys. Rev. B* **27**, 112–118 (1983).
- [54] T. Wegehaupt and R. E. Doezema, “Measurement of the anisotropic Fermi velocity in Al,” *Phys. Rev. B* **16**, 2515 (1977).
- [55] N. A. Mortensen, K. Flensberg, and A.-P. Jauho, “Angle dependence of Andreev scattering at semiconductor–superconductor interfaces,” *Phys. Rev. B* **59**, 10176–10182 (1999).
- [56] The width of the V_{dc} range corresponding to the superconducting gap becomes narrower at low fields due to the increasing bulk conductivity near the S/Sm junction.
- [57] The only reports are for the setups of crossed Andreev reflection [12, 18].
- [58] The consistency of the model can be checked by seeing that $T_l = 1$ and $P_h = 0.5$ give $R_d = 0$ and $R_u = 1/\nu G_0$ as expected for the conventional QH effects with normal contacts, while $T_l = 1$ and $P_h = 1$ give $R_d = -1/2\nu G_0$ and $R_u = 1/2\nu G_0$ as expected for perfect Andreev reflection.
- [59] L. Arrachea, A. L. Yeyati, and C. A. Balseiro, “Signatures of triplet superconductivity in $\nu = 2$ chiral Andreev states,” *Phys. Rev. B* **109**, 064519 (2024).
- [60] J. A. M. van Ostaay, A. R. Akhmerov, and C. W. J. Beenakker, “Spin-triplet supercurrent carried by quantum Hall edge states through a Josephson junction,” *Phys. Rev. B* **83**, 195441 (2011).
- [61] O. Gamayun, J. A. Hutasoit, and V. V. Cheianov, “Two-terminal transport along a proximity-induced superconducting quantum Hall edge,” *Phys. Rev. B* **96**, 241104 (2017).
- [62] D.-L. Nguyen, C.-M. Wei, and M.-Y. Chou, “Theoretical study of quantum size effects in thin Al(100), Al(110), and Al(111) films,” *Phys. Rev. B* **99**, 205401 (2019).
- [63] T. D. Stanescu and S. Das Sarma, “Proximity-induced superconductivity generated by thin films: Effects of Fermi surface mismatch and disorder in the superconductor,” *Phys. Rev. B* **106**, 085429 (2022).
- [64] B. J. van Wees, G. I. Meijer, J. J. Kuipers, T. M. Klapwijk, W. van de Graaf, and G. Borghs, “Breakdown of the quantum Hall effect in InAs/AlSb quantum wells due to counterflowing edge channels,” *Phys. Rev. B* **51**, 7973–7976 (1995).
- [65] T. Akiho, H. Irie, K. Onomitsu, and K. Muraki, “Counterflowing edge current and its equilibration in quantum Hall devices with sharp edge potential: Roles of incompressible strips and contact configuration,” *Phys. Rev. B* **99**, 121303 (2019).
- [66] S. Komatsu, H. Irie, T. Akiho, T. Nojima, T. Akazaki, and K. Muraki, “Gate tuning of fractional quantum Hall states in an InAs two-dimensional electron gas,” *Phys. Rev. B* **105**, 75305 (2022).